

Demonstration of a large-scale optical exceptional point structure

Liang Feng,¹ Xuefeng Zhu,^{1,2} Sui Yang,^{1,3} Hanyu Zhu,¹ Peng Zhang,¹ Xiaobo Yin,^{1,3} and Yuan Wang,^{1,3} and Xiang Zhang^{1,3,*}

¹National Science Foundation Nanoscale Science and Engineering Center, 3112 Etcheverry Hall, University of California, Berkeley, CA 94720, USA

²Huazhong University of Science and Technology, Wuhan, Hubei 430074, China

³Materials Sciences Division, Lawrence Berkeley National Laboratory (LBNL), 1 Cyclotron Road, Berkeley, CA 94720, USA

*xiang@berkeley.edu

Abstract: We report a large-size (4-inch) optical exceptional point structure at visible frequencies by designing a multilayer structure of absorbing and non-absorbing dielectrics. The optical exceptional point was implemented as indicated by the realized unidirectional reflectionless light transport at a wafer scale. The associated abrupt phase transition is theoretically and experimentally confirmed when crossing over the exceptional point in wavelengths. The large scale demonstration of phase transition around exceptional points will open new possibilities in important applications in free space optical devices.

©2013 Optical Society of America

OCIS codes: (310.4165) Multilayer design; (310.6845) Thin film devices and applications.

References and links

1. M. A. Kats, R. Blanchard, P. Genevet, and F. Capasso, "Nanometre optical coatings based on strong interference effects in highly absorbing media," *Nat. Mater.* **12**(1), 20–24 (2013).
2. C. M. Bender and S. Böttcher, "Real spectra in non-Hermitian Hamiltonians having PT symmetry," *Phys. Rev. Lett.* **80**(24), 5243–5246 (1998).
3. K. G. Makris, R. El-Ganainy, D. N. Christodoulides, and Z. H. Musslimani, "Beam dynamics in PT symmetric optical lattices," *Phys. Rev. Lett.* **100**(10), 103904 (2008).
4. S. Klaiman, U. Günther, and N. Moiseyev, "Visualization of branch points in PT -symmetric waveguides," *Phys. Rev. Lett.* **101**(8), 080402 (2008).
5. C. E. Rüter, K. G. Makris, R. El-Ganainy, D. N. Christodoulides, M. Segev, and D. Kip, "Observation of parity-time symmetry in optics," *Nat. Phys.* **6**(3), 192–195 (2010).
6. Z. Lin, H. Ramezani, T. Eichelkraut, T. Kottos, H. Cao, and D. N. Christodoulides, "Unidirectional invisibility induced by PT -symmetric periodic structures," *Phys. Rev. Lett.* **106**(21), 213901 (2011).
7. A. Regensburger, C. Bersch, M. A. Miri, G. Onishchukov, D. N. Christodoulides, and U. Peschel, "Parity-time synthetic photonic lattices," *Nature* **488**(7410), 167–171 (2012).
8. L. Feng, Y. L. Xu, W. S. Fegadolli, M. H. Lu, J. E. B. Oliveira, V. R. Almeida, Y. F. Chen, and A. Scherer, "Experimental demonstration of a unidirectional reflectionless parity-time metamaterial at optical frequencies," *Nat. Mater.* **12**(2), 108–113 (2013).
9. S. Longhi, "PT-symmetric laser absorber," *Phys. Rev. A* **82**(3), 031801 (2010).
10. Y. Choi, S. Kang, S. Lim, W. Kim, J. R. Kim, J. H. Lee, and K. An, "Quasieigenstate coalescence in an atom-cavity quantum composite," *Phys. Rev. Lett.* **104**(15), 153601 (2010).
11. S. B. Lee, J. Yang, S. Moon, S. Y. Lee, J. B. Shim, S. W. Kim, J. H. Lee, and K. An, "Observation of an exceptional point in a chaotic optical microcavity," *Phys. Rev. Lett.* **103**(13), 134101 (2009).
12. C. Dembowski, H. D. Gräf, H. L. Harney, A. Heine, W. D. Heiss, H. Rehfeld, and A. Richter, "Experimental observation of the topological structure of exceptional points," *Phys. Rev. Lett.* **86**(5), 787–790 (2001).
13. J. G. Muga, J. P. Palao, B. Navarro, and I. L. Egusquiza, "Complex absorbing potentials," *Phys. Rep.* **395**(6), 357–426 (2004).
14. F. Cannata, J. P. Dedonder, and A. Ventura, "Scattering in PT -symmetric quantum mechanics," *Ann. Phys.* **322**(2), 397–433 (2007).
15. W. D. Heiss, "Exceptional points of non-Hermitian operators," *J. Phys. Math. Gen.* **37**(6), 2455–2464 (2004).
16. H. Cartarius, J. Main, and G. Wunner, "Exceptional points in atomic spectra," *Phys. Rev. Lett.* **99**(17), 173003 (2007).
17. L. Ge, Y. D. Chong, and A. D. Stone, "Conservation relations and anisotropic transmission resonances in one-dimensional PT -symmetric photonic heterostructures," *Phys. Rev. A* **85**(2), 023802 (2012).

18. N. Liu, M. Mesch, T. Weiss, M. Hentschel, and H. Giessen, "Infrared perfect absorber and its application as plasmonic sensor," *Nano Lett.* **10**(7), 2342–2348 (2010).
19. Y. Cui, K. H. Fung, J. Xu, H. Ma, Y. Jin, S. He, and N. X. Fang, "Ultrabroadband light absorption by a sawtooth anisotropic metamaterial slab," *Nano Lett.* **12**(3), 1443–1447 (2012).

1. Introduction

Optical losses are responsible for power attenuation, and thus typically degrade the performance of optical devices. Consequently, conventional optical devices are usually made of non-absorbing transparent dielectric materials. Most recently, it has been suggested that the use of highly-absorbing dielectrics could result in intriguing optical phenomena [1]. If material losses are further designed intercorrelated with the index of refraction, unique optical functionalities can be expected. Judiciously designed photonic synthetic matters, which take advantage of optical losses by engineering the entire complex dielectric permittivity plane, may be investigated to mimic the complex non-Hermitian Hamiltonians in quantum mechanics [2] and thus realize unique directional light transport and novel devices [3–9] at the parity-time phase transition point, a type of exceptional points. However, exceptional point is much more general concept, contains broader and richer physics, and should thus be expected in a larger non-Hermitian family: exceptional points are singularities in the complex eigen spectrum and inherently associated with degenerate eigen states, leading to a series of interesting physical effects including level repulsion and crossing, bifurcation and chaos, as well as phase transition in a number of open quantum system configurations [10–12].

In this work, driven by the unique transport behaviors enabled by non-Hermiticity, we exploited absorbing dielectric materials such as silicon (Si) to achieve a large size planar optical structure with an exceptional point at visible frequencies. Instead of minimizing optical losses, we intentionally utilized the losses together with the modulated index of refraction. By engineering their interplay, we developed a 4-inch sized multilayer exceptional structure and demonstrated its associated accidental degeneracy at the exceptional point. The implemented exceptional point also accounted for an abrupt change in the generalized power spectrum observed experimentally, manifesting a phase transition at a wafer scale. Moreover, because of the intrinsic planar configuration, our exceptional point structure is highly scalable in fabrication and can be implemented in both micro- and macro-scale applications.

2. Exceptional point and phase transition

Similar to the Hamiltonian matrix in quantum mechanics, light propagation in a dielectric medium can be described using the corresponding optical scattering matrix, which relates the initial state and the final state of an optical system. Here, for simplicity in the design, we will

consider a two-port optical system whose scattering matrix is described as $S = \begin{pmatrix} t & r_b \\ r_f & t \end{pmatrix}$ [12–

14], where t is the transmission coefficient, r_f and r_b are reflection coefficients in forward and backward directions, respectively. As quantum exceptional points are designed by engineering the Hamiltonian matrix [10], optical exceptional points can be achieved by manipulating the elements in the corresponding optical scattering matrix. The corresponding eigen values of the studied two-port system are $s_n = t \pm \sqrt{r_f r_b}$. As stated above, the desired optical exceptional point require the realization of degeneracy of two eigen values of such an optical system. Apparently, two eigen values become degenerate to form exceptional points in the complex eigen spectrum when either r_f or r_b is zero, i.e., the system is unidirectional reflectionless.

Here, we will design and demonstrate a general optical exceptional point rather than the special parity-time phase transition point in a large-scale free space device. A multilayer structure consisted of absorbing and non-absorbing dielectrics at visible frequencies, i.e., amorphous Si and silica, respectively [Fig. 1(a)], to tailor the asymmetric optical response. Each unit cell consisted of 4 alternating thin film layers of Si and silica (23 nm Si/ 26 nm silica/ 9 nm Si/43 nm silica).

In this multi-layer system, light propagation in each layer j can be described by the matrix

$$M_j = \begin{pmatrix} \cos k_j L_j & \frac{1}{k_j} \sin k_j L_j \\ -k_j \sin k_j L_j & \cos k_j L_j \end{pmatrix}, \quad j = 1, 2, \dots, N \quad (1)$$

where k_j is the corresponding wave number, L_j the thickness of the layer, and N is the total number of layers. It is worth noting that this transfer matrix method is valid for the 1-dimensional system, so in the design we assume each layer is infinite in the transverse dimensions. Therefore the transfer matrix of the entire system can be written as $M^f = M_N \cdot \dots \cdot M_2 \cdot M_1$ for light propagating in the forward direction from layer 1 to layer N . The corresponding transmission and reflection coefficients can be derived:

$$t = 2ik_0 e^{-ik_0 L} \left[\frac{M_{11}^f M_{22}^f - M_{12}^f M_{21}^f}{-M_{21}^f + k_0^2 M_{21}^f + ik_0 (M_{11}^f + M_{22}^f)} \right] \quad (2)$$

and

$$r_f = \left[\frac{(M_{21}^f + k_0^2 M_{12}^f) + ik_0 (M_{22}^f - M_{11}^f)}{(-M_{21}^f + k_0^2 M_{12}^f) + ik_0 (M_{22}^f + M_{11}^f)} \right], \quad (3)$$

where L is the total thickness of the multi-layer system and k_0 is the wave vector in free space. When light is propagating in the backward direction, the transfer matrix then becomes $M^b = M_1 \cdot \dots \cdot M_{N-1} \cdot M_N$. The corresponding reflection coefficient can be derived accordingly:

$$r_b = \left[\frac{(M_{21}^b + k_0^2 M_{12}^b) + ik_0 (M_{22}^b - M_{11}^b)}{(-M_{21}^b + k_0^2 M_{12}^b) + ik_0 (M_{22}^b + M_{11}^b)} \right]. \quad (4)$$

The desirable unidirectional characteristics ($r_f = 0$) was accomplished at the wavelength of 532 nm by simultaneously engineering the thickness of Si and silica layers according to Eqs. (1)–(4), such that the accumulated phase change in both layers is in-phase correlated with absorption due to the imaginary part of the refractive index of Si. The absorption of Si layers caused strong attenuation in transmission. Although transmissions are the same in both directions, the multilayer structure shows significant direction-dependent response in reflection. In the forward direction, light constructively interferes in the Si layers but destructively interferes at the top surface of the structure, leading to a zero reflection coefficient in the complex plane with strong absorption in the structure; while in the backward direction, light is mainly confined in the silica layers with a destructive interference at the bottom surface of the structure, resulting in high reflection. Although single unit cell is unidirectional reflectionless by itself, the structure in the design comprises 4 periodic unit cells to further enhance the backward reflection, while still keeping the forward reflection zero. Compared to the previously studied parity-time symmetric optical materials [5,7,8], the geometry of our current exceptional point structure is less complicated for implementing the optical exceptional point and can be performed using the well-developed thin-film techniques.

To gain deeper insight into the exceptional point, we analytically derived the scattering matrix [13–15] and its modified form [8] to investigate the scattering behaviors of the system. A multi-valued Riemann surface as a spectrum of complex eigenvalues of the modified scattering matrix [Fig. 1(b)] was calculated to represent two eigen branches $s_n = t \pm \sqrt{r_f r_b}$. Two branches of the Riemann surface represent two superposition states between forward and backward light scatterings including both transmission and reflection. By varying the

imaginary part of the refractive index of Si, the solutions of two branches coalesce and lead to two exceptional points, corresponding to two singularity points in the complex Riemann surface that are phase conjugates to each other. At the exceptional points, light scattering is a destructive interference of two branch solutions depicted by two sheets of the Riemann surface. Consequently, the corresponding modal interference at the exceptional points suppresses the reflection in either the forward or backward direction. This was validated by the finite element method simulations at the exceptional point with $\text{Im}(n_{\text{Si}}) = -0.65$ [Fig. 1(c)] where the experiment was performed. The corresponding amplitude and phase diagrams in the device are shown in Figs. 1(d) and 1(e), respectively, showing strong field confinement in the Si layers in the forward direction and thus leading to zero forward reflection.

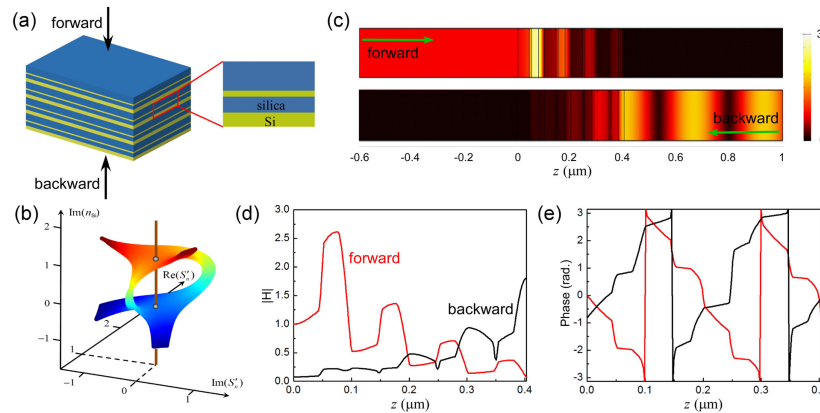


Fig. 1. (a) Schematic of the optical exceptional point structure on a glass wafer designed at the wavelength of 532 nm, where $n_{\text{Si}} = 4.86 - j0.65$ and $n_{\text{silica}} = 1.46$. (b) Complex eigen value solutions of the modified scattering matrix at 532 nm construct a multi-valued Riemann surface as a function of $\text{Im}(n_{\text{Si}})$, where red color indicates optical gain and blue corresponds to absorption as we have in Si layers. (c) Simulations of light propagating through the exceptional point structure in the forward (upper panel) and backward (lower panel) directions, in which the distribution of the amplitude of the magnetic field is shown normalized to the incident magnetic field of 1. (d) and (e) are amplitude and phase of the magnetic field in the device as light propagate in the forward (red) and backward (black) directions, respectively.

Because of the associated accidental degeneracy, exceptional points are typically responsible for bifurcation and phase transition in open quantum systems [10,16]. In our structure, the optical exceptional point also experiences a phase transition as a function of wavelengths according to the generalized power representation $T + \sqrt{R_f R_b}$ [17], where $T = |t|^2$ is transmittance, and $R_f = |r_f|^2$ and $R_b = |r_b|^2$ are reflectance in forward and backward directions, respectively. The generalized power relates all the elements in the scattering matrix and represents the power summation of superpositions of the two eigen states derived from the scattering matrix. According to Eqs. (2)–(4), the generalized power spectrum and its differential spectrum can be obtained as shown in Fig. 2, in which material dispersions are also considered in calculations. Here, wavelength detuning is defined as $\Delta = \lambda - \lambda_{EP}$, where λ_{EP} corresponds to the designed exceptional point wavelength where reflection is forward reflectionlessness. It is evident that, as shown in Fig. 2(a), the exceptional point ($\Delta = 0$) divides the generalized power spectrum into two phases: a power-decreasing phase at $\Delta < 0$ and the other with increasing generalized power at $\Delta > 0$. Moreover, the differential generalized power spectrum manifests an abrupt phase change at the exceptional point [Fig. 2(b)], which resembles the classical solid-liquid phase transition in which the derivative of the Gibbs free energy on temperature is discontinuous at the transition point. These results originate from the realized optical exceptional point as well as its associated level crossing. If

crossing over the exceptional point in any parameter axis such as wavelengths in our case, optical phase of reflected light undergoes an abrupt π phase jump, similar to the phase transition from the parity-time symmetric phase to the parity-time broken phase in the parity-time symmetric systems, in which the chosen parameter axis is the amplitude of the imaginary part of the index modulation [5–8].

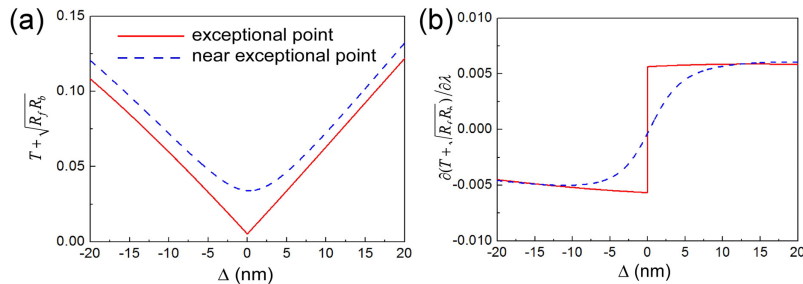


Fig. 2. (a) and (b) are calculated spectra of generalized total power and its partial derivatives as a function of wavelength detuning. The red curves denote the spectra with the exact exceptional point design, while the blue dash curves are the case near the exceptional point.

3. Experimental validation

The 4-inch exceptional point structure was fabricated by alternating thin film depositions of amorphous Si and silica layers on a cleaned glass wafer using plasma enhanced chemical vapor deposition (PECVD) [Fig. 3(a)]. Although the PECVD process is not able to realize atomically flat thin films as we assumed in analysis and simulations, the resulted non-uniformity is on the order of nanometers, which is so small that light still “sees” flat thin films when propagating through.

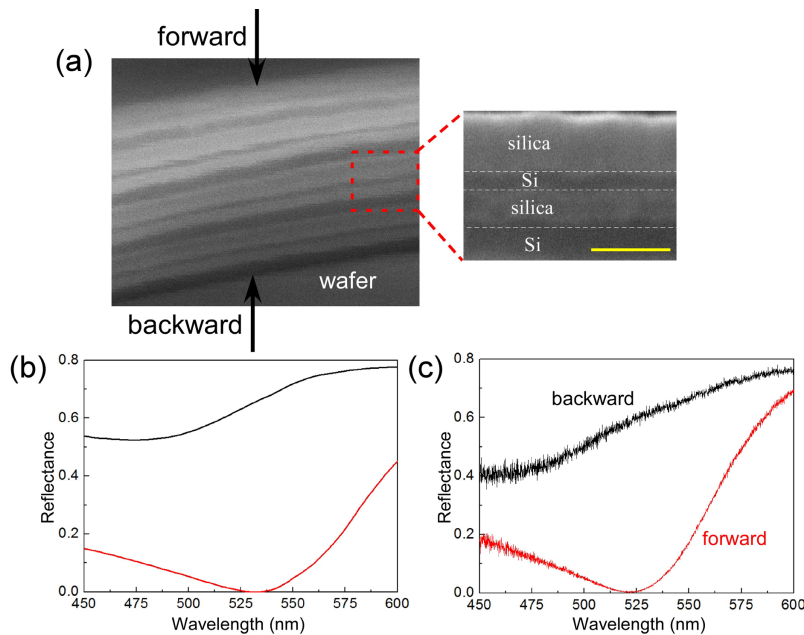


Fig. 3. (a) SEM pictures of the cross-section of the fabricated exceptional point structure. Scale bar, 50 nm. (b) and (c) are numerically calculated and experimentally measured reflection spectra of the exceptional point structure from 450 nm to 600 nm, respectively, for both forward (red) and backward (black) incidence.

The reflection spectra of the structure for both forward and backward directions were numerically calculated and experimentally measured, as shown in Figs. 3(b) and 3(c), respectively. The results consistently showed that with normal incident light, reflection spectra in forward and backward directions are in significant contrast within the spectral range of interest. The unidirectional reflectionless light transport was clearly demonstrated around the wavelength of 520 nm in measurements, where reflection in the forward direction was diminished owing to the implemented exceptional point. The small discrepancy between the calculations and experiments may result from the imperfect control of the film thickness in the PECVD process. Additionally, the PECVD Si films may contain less absorption because of the hydrogenation in the process compared to the index used in the calculations.

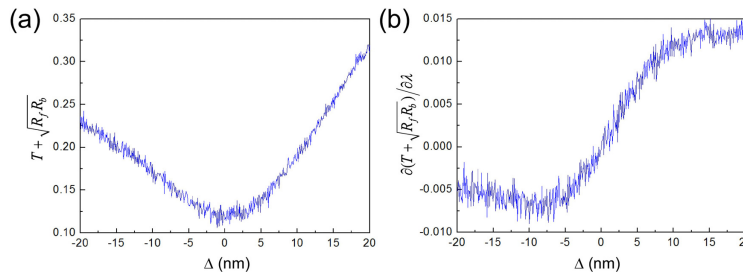


Fig. 4. Experimentally measured generalized power spectrum (a) and its differential spectrum (b) around the exceptional point.

With the data in Fig. 3(c), the experimentally measured generalized power spectrum and its differential one can be derived as shown in Fig. 4. Phase transition from decreasing power to increasing power can be clearly observed around the exceptional point [Fig. 4(a)], but the transition in the differential spectrum is not as abrupt as predicted in Fig. 2(b). The fact that the spectrum in Fig. 4(b) is still differential at $\Delta = 0$ is because it is difficult to exactly reach the exceptional point in experiments owing to its inherent singularity. The designed exceptional point requires the implemented geometry parameters to exactly match the design, which is hard to achieve in experiments. For example, the absorption of the PECVD Si film is typically smaller and thin film thickness may slightly vary in the fabrication. However, even though the structure parameters are slightly off the exceptional point (see Fig. 2 for the case near the exceptional point in which we considered lower absorption for Si films with $\text{Im}(n_{\text{Si}}) = -0.6$), $\Delta = 0$ still divides the generalized power spectrum into two phases and the drastic phase change in the differential power spectrum can be convincingly observed in both experiments and calculations, though the slope in the generalized power spectrum at $\Delta > 0$ is different than that in calculations (Fig. 2) due to the imperfect PECVD fabrication. It is expected that the transition becomes sharper when it is even closer to the exceptional point.

Moreover, the planar configuration of our exceptional point structure allows light incoming from a wide angular spectrum for imaging, further distinguished than the previous waveguide implementations where light is limited to only the normal incidence by waveguides. Because of the associated unidirectional light propagation at the exceptional point, the coated glass wafer can form imaging in reflection only for backward propagating light under sunlight illumination, as shown in Fig. 5 in which photographs of the wafer were taken from both sides using a cellular phone camera. The corresponding reflection vanished in the forward direction [Fig. 5(a)], while an image was clearly photographed in the backward direction [Fig. 5(b)]. By applying the transfer matrix method in which the matrix is modified corresponding to the incident angle and polarization, the reflection spectra for oblique incidence can be obtained. Therefore, angular dependence of the reflection spectra was investigated by varying the incident angles at the exceptional point wavelength in both calculations [Fig. 5(c)] and measurements [Fig. 5(d)]. Under unpolarized light illumination reflections in both directions were not angle sensitive. However, the modifications in the transfer matrix cause the disappearance of the degeneracy of the scattering matrix for the non-

zero incident angles as two eigen branches cannot coalesce in the parameter space shown in Fig. 1(b). Although light propagation in the forward direction was not perfectly reflectionless at oblique incidence, the large reflection contrast in both directions existed in a wide angular spectrum. Therefore, our structure may enable perfect absorption at the exceptional point for forward propagating light in a relatively large angular spectrum if the structure is thick enough to significantly attenuate transmitted light as implemented in the current experiment. Although similar effects was observed before, the physics behind our structure is completely different: the demonstrated forward reflectionlessness forms an exceptional point, while in the past perfect absorption structures [1,18,19], reflection is small but cannot exactly reach zero such that two eigen values of the scattering matrix do not degenerate and no exceptional point exists. Consequently, the demonstrated abrupt phase transition around the exceptional point cannot be expected in those structures. It is also worth noting that even with only 1 unit cell in Fig. 1(a), forward reflection would diminish in our structure and thus the same exceptional point still exists in the complex eigen spectrum.

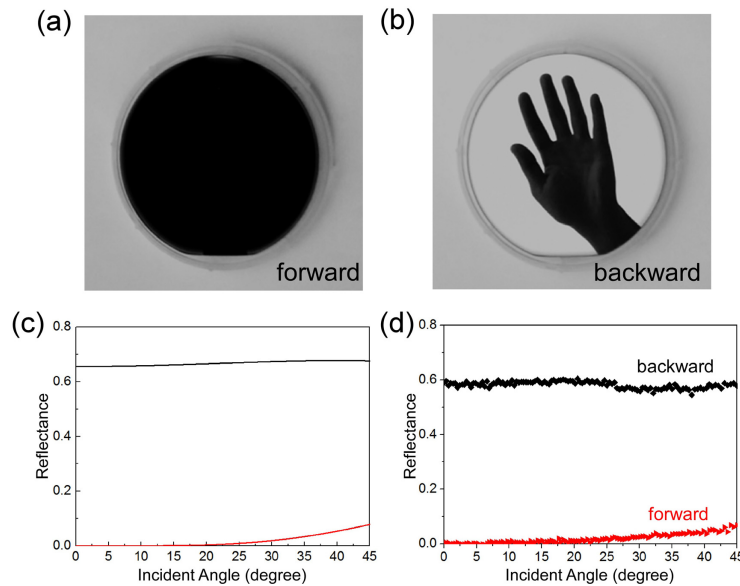


Fig. 5. (a) and (b) are photographs of the wafer-scale exceptional point structure in forward and backward directions, respectively with a 10 nm band pass filter centered at the wavelength of 520 nm. (c) and (d) show numerically and experimentally the angular dependence of reflection spectra of unpolarized light at the exceptional point in both forward (red) and backward (black) directions for incident angle from 0 to 45°. The reflectance for non-zero incident angle is the corresponding intensity of light at the reflection angle symmetric to the incident angle with respect to the normal.

4. Conclusion

We experimentally realized, for the first time, a 4-inch wafer-scale exceptional point structure and its associated phase transition at visible frequencies. The demonstrated exceptional point and the phase transition around it originate from the singularity in the complex eigen spectrum. In fact, exceptional points are generally intrinsic to open quantum systems and can thus be expected in a large family of non-Hermitian Hamiltonians [10–16]. Therefore, sophisticated engineering of optical losses is expected to mimic a variety of quantum phenomena in the optical regime and enable a series of unique optical functionalities. Moreover, because of the occurrence of the phase transition, the dynamic change of the hidden topology can be observed in the vicinity of the exceptional points [12], giving rise to geometric phase and providing great flexibility for manipulating physical responses. More importantly, in contrast to all the previous experimental studies in delicate optical parity-time

symmetric systems [5,7,8], the demonstrated wafer-scale implementation of optical exceptional points and phase transition, for the first time, in our multilayer structure confirmed the feasibility of realizing complicated non-Hermitian light transport to develop a new generation of free space optical devices.

Acknowledgments

This work was supported by the U.S. Department of Energy, Basic Energy Sciences Energy Frontier Research Center (DoE-LMI-EFRC) under award DOE DE-AC02-05CH11231.